

The Potential of *Clerodendrum paniculatum* Leaves Fraction as a 3-Chymotrypsin-Like (3CL) Protease Inhibitor of SARS-CoV-2

Muhammad Arba^{1*}, Arfan Arfan¹, Yamin Yamin¹, and Muhammad Sulaiman Zubair²

¹Faculty of Pharmacy, Halu Oleo University, Kendari 93232, Indonesia

²Faculty of Pharmacy, Tadulako University, Palu 94148, Indonesia

* **Corresponding author:**

email: muh.arba@uho.ac.id

Received: January 18, 2023

Accepted: March 3, 2023

DOI: 10.22146/ijc.81447

Abstract: We described the biological activity of the *Clerodendrum paniculatum* leaf fraction against the SARS-CoV-2 3-Chymotrypsin-like 3CL protease at the molecular level. This study applied LC-MS/MS to identify bioactive compounds from fractions, computational studies, and fluorescence resonance energy transfer (FRET) assays to ascertain their inhibitory activity. LC-MS/MS analysis of the three samples revealed that sample 1 contained 18 compound peaks. In samples 2 and 3, there were 23 and 25 compounds with different molecular weights, respectively. Docking's study identified that the alkaloids (komarovicine and roemerine) have lower binding energies than other metabolites and standard compounds, with values of -33.47 and -32.63 kJ/mol, respectively. Roemerine demonstrated excellent stability based on dynamic simulation results and confirmed its affinity for 3CL protease predicted by the MM-PBSA approach of -89.44 kJ/mol. The FRET method for testing 3CL protease activity revealed that sample 2 had an enzyme inhibitory activity of 94.3%, which was close to that of GC376 (98.19%). Meanwhile, samples 1 and 3 yielded satisfactory inhibition activity by 89.64% and 85.24%, respectively. The antiviral activity of *C. paniculatum* leaves was discovered for the first time by inhibiting the 3CL protease SARS-CoV-2, providing an excellent opportunity for its development as an anti-SARS-CoV-2.

Keywords: *Clerodendrum paniculatum*; COVID-19; molecular dynamics simulation; SARS-CoV-2; 3-chymotrypsin-like protease

■ INTRODUCTION

COVID-19 has been a pandemic since it first spread from the capital of Hubei Province, Wuhan, at the end of 2019 [1]. Coronavirus disease reduces the function of the human respiratory system owing to infection with SARS-CoV-2 and has spread worldwide [2]. Efforts to deal with this virus globally are being vigorously carried out [3]. However, the pathogen transmission rate is swift, and the effectiveness of therapy needs to be increased [4]. The therapeutic management of COVID-19 patients needs to be improved and limited [5]. Various clinical trials are underway, including remdesivir, lopinavir/ritonavir, favipiravir, and hydroxychloroquine combined with azithromycin as alternatives to solve this problem [6-8]. Several studies have shown ineffective results and adverse side effects associated with these drugs [9-10]. Based on

this information, new drug candidates to inhibit this coronavirus urgently need to improve treatment strategies for COVID-19 patients.

The search for SARS-CoV-2 inhibitors against critical targets such as papain-like protease, helicase, RNA-dependent RNA polymerase, uridine-specific endonuclease, and 3-Chymotrypsin-like proteases has become a focus of research due to their vital functions [11-13]. These targets are responsible for protein synthesis, viral replication, and viral infection [14-15]. The 3CL protease is a promising target. In addition to its role in viral replication, it is responsible for the conserved catalytic site cleavage mechanism in SARS-CoV-2 polyproteins 1a (pp1a) and 1ab (pp1ab) [16]. The translation of the coronavirus replication gene produces these two polyproteins. Pp1a modifies host cell factors

and aids in the preparation of cells for viral RNA synthesis, whereas pp1ab catalyzes and regulates viral RNA replication and transcription [17-18]. Viral replication can be completely inhibited by inhibiting this proteolytic process, virus replication can be completely stopped [19].

Natural products offer great opportunities in the pharmaceutical sector because they are lead compounds in various modern medicines [20]. Natural products contain unique compounds and diverse structures with pharmacological properties that contribute to drug discovery and development [21]. One of the natural products reported to be practical in traditional medicine and proven to have various biological activities is *C. paniculatum* [22]. In Indonesia, especially in the Central Buton Regency, Southeast Sulawesi Province, *C. paniculatum* is known as Kamena-mena. *C. paniculatum* has biological activity as antioxidant, anticancer, hepatoprotective, anti-inflammatory, antimicrobial, antimutagenic, antiaging, anthelmintic, hypolipidemic, and insecticidal [23-25]. There are few reports on the antiviral activity of this plant. Several families of *Clerodendrum*, such as *C. myricoides*, have antiviral activity against HIV and respiratory syncytial virus (RSV), which cause bronchitis and pneumonia [26]. In addition, based on *in silico* studies, oleanolic acid, and acetoside compounds from *C. serratum* were thought to inhibit the main proteases, NSP3 and NSP15 of SARS-CoV-2 [27]. Therefore, this study aimed to investigate the antiviral activity of the *C. paniculatum* leaf fraction through inhibition of the 3CL protease SARS-CoV-2 in an *in vitro* assay. Lastly, the mechanism at the molecular level of the identified compounds in this fraction was explained using LC-MS/MS combined with an *in silico* study to reveal its potential as an anti-COVID-19 agent.

■ EXPERIMENTAL SECTION

Materials

Fresh leaves of *C. paniculatum* were collected from the middle of the Masangka sub-district, Buton Tengah district, Southeast Sulawesi Province, Indonesia. Fresh leaves were washed with running water, stoned, and dried in the sun. The sample was covered with a black cloth to avoid direct contact with ultraviolet light during drying.

Procedure

Extraction

Dried *C. paniculatum* leaves were ground using an electric blender (SHARP®) at 240 W to obtain a fine powder. The maceration method was applied for the extraction process, in which 800 g of *C. paniculatum* leaf powder was immersed in 8 L ethanol. Maceration was carried out at room temperature for 3 × 24 h and filtered every 1 × 24 h with Whatman paper Number 1 [28]. A rotary evaporator was used to concentrate the filtrate at 40 °C to obtain a thick extract of 102 g.

Fractionation

A vacuum column chromatography method with a solvent gradient system was used for fractionation. The eluent was a mixture of *n*-hexane and ethyl acetate to obtain the polar, semipolar, and nonpolar fractions. The fractionation results were separated into three categories: samples 1, 2, and 3. Sample 1 was eluted with *n*-hexane: ethyl acetate (100:0 to 70:30 mL). Sample 2 was followed by solvent *n*-hexane: ethyl acetate at a ratio of 60:40 to 30:70 mL. Sample 3 was eluted with *n*-hexane: ethyl acetate at a ratio of 20:80 to 0:100 mL. Finally, the samples were cleaned with 100 mL ethanol.

LC-MS/MS analysis

Each *C. paniculatum* sample was injected into the column with a 1 mL aliquot at a flow rate of 0.3 mL/min. Instrument adjustments were as follows: gain time 0.00–16.00 min, initial mass 50.00–120.00 *m/z*, low collision energy, 6 eV; high energy 10–40 eV, ESI acquisition mode (+); capillary and conical voltages were set at 2 kV and 30 V. The cone and desolvation gas flow rates were 50 and 1000 L/h. The temperature was adjusted to 500 °C for desolvation, 120 °C for source, 40 °C for column, and 20 °C for sample. The resulting data were processed using UNIFI software (version 1.8, Waters Corporation, Milford, Massachusetts, MA, USA) and matched against a database of compounds based on molecular weight, molecular formula, and chemical structure.

Molecular docking stage

The crystal structure of the SARS-CoV-2 3CL protease with code 6M2N (<https://www.rcsb.org/>) was

chosen for the molecular docking stage [29]. First, the crystallized water molecules and bound ligands were removed from the receptor utilizing AutoDock Tools version 1.5.6 [30]. The protease structure was prepared by adding polar hydrogen atoms and Kollman charges. Finally, the protease was generated in the PDBQT format [31]. The 3D structures of all compounds identified in the LC/MS-MS analysis were collected from the PubChem database (<https://pubchem.ncbi.nlm.nih.gov/>). All compounds were released under restraint and assigned Gasteiger charges with the assistance of the AutoDock Tools program. The docking process utilized AutoDock Vina software [32]. The grid box area was arranged according to the position of baicalein (the reference ligand) on the protease. The grid coordinates were set at -32,981; -65,438; and 41,404 for the x, y, and z axes with an area length of 50 Å. The best compounds and their interactions with the 3CL protease from the docking results were analyzed using Discovery Studio Visualizer.

Molecular dynamic simulation

The best compounds from the docking results were subjected to molecular dynamics simulations using GROMACS 2016 software to determine their stability [33]. The AMBER99SB-ILDN and GAFF force fields for the protein and ligand, respectively, were used in the simulation [31,34]. ACPYPE was used to create parametric ligands [35]. The TIP3P water model was then applied to solve each system, with a minimum distance of 10 Å around the complex and neutralized with Na⁺ and Cl⁻ ions. Three phases were performed successively to complete the minimization step, each of which had conjugate gradients of 5,500 steps and the steepest descents of 500 steps. Every 50 ps, each complex was gradually heated to 310 K in an NVT ensemble with a time step of 0.0005 ps [36]. The system was relaxed using NPT's 500 ps equilibration steps, and production was run with a 2 fs timestep for a 100 ns simulation. The particle mesh Ewald method was used to mimic electrostatic interactions and rectify the 1.2 nm cut-off for van der Waals energy terms [37]. The stability of the complexes was verified by analyzing the root-mean-square deviation (RMSD), root-mean-square fluctuation (RMSF), radius gyration (Rg), and principal component analysis (PCA) parameters. The

complex's binding energy was calculated using the MM/PBSA method [38]. High-Performance Computing (HPC) hardware was used for the docking and dynamic simulations, with Intel (R) Core i5-8500 processor specifications @4.30 GHz (6 CPUs), 4096 MB RAM, 2 TB hard drive, 120 GB solid-state drive, and VGA Intel HD Graphics NVIDIA GeForce GTX 1080 Ti.

FRET-based in vitro assay on 3CL protease of SARS-CoV-2

The *in vitro* assay was performed following the procedure which was reported in our previous research [39]. Approximately 12 µL of dithiothreitol (0.5 M) was added to 6 mL of buffer to prepare the assay buffer. The dilution process was carried out by adding an assay buffer of 3.95 mL for the enzyme and 950 µL for the substrate. The sample was dissolved in DMSO at a concentration of 500 µM (200 µg/mL) in a 96-well microplate. The control inhibitor was GC376, a peptidomimetic made at the same concentration as the sample. Then, 12 µL of dithiothreitol with a concentration of 0.5 M was added to 6 mL of buffer to prepare the assay buffer. The dilution process was carried out by adding an assay buffer of 3.95 mL for the enzyme and 950 µL for the substrate. Ten microliters of the sample and control (GC376) were added to 30 µL of each enzyme (5 ng/µL) to produce a mixed volume of 40 µL. The mixture was then incubated at 25 °C for 30 min with gentle shaking. Finally, 10 µL of the substrate (250 µM) was added. The mixture was then incubated for 1 × 24 h and absorbance was measured at a wavelength 360/460 nm with a Synergy HTX-3 Multi-mode Reader (Winooski, Vermont, VT, USA).

RESULTS AND DISCUSSION

LC-MS/MS Analysis

LC-MS/MS succeeded in recognizing several compounds in the *C. paniculatum* fraction based on the molecular mass and similarity in retardation time in the database of UNIFI 1.8 software. In sample 1, 18 peaks were observed (Table 1). The results for samples 2 and 3 revealed 23 and 25 peaks, respectively (Table 2 and 3). Each peak indicated the presence of a compound with a specific molecular weight. The same compounds, such

as yohimbic acid and convolidine, were found in all the samples. However, compounds found in only one sample were also observed, such as 2,4-dihydroxy acetophenone in sample 1, glycocitridine in sample 2, and 9,10,16-trihydroxy hexadecanoic acid, alpha-dihydrolysergol, and ajmaline in sample 3.

Table 1. The LC-MS/MS analysis of sample 1 of *C paniculatum*

Peak	<i>m/z</i>	Identified Compound
1	137.3090	-
2	197.4042	-
3	340.5990	Yohimbic acid/ Behenic acid
4	397.1448	-
5	453.6928	-
6	274.5595	-
7	288.5544	Testosterone
8	277.4959	Convolidine/Venlafaxine
9	279.5576	Roemerine
10	353.5950	Trichodesmine
11	313.6079	Heliotrine
12	299.6129	Komarovicine
13	429.5112	-
14	607.6002	-
15	152.3011	2,4-Dihydroxyacetophenone/2,6-Dihydroxyacetophenone/2-Mercaptopurine/6-Mercaptopurine/o-Anisic acid/Ribitol/Vanilin
16	405.7049	-

Table 2. The LC-MS/MS analysis of sample 2 of *C. paniculatum*

Peak	<i>m/z</i>	Identified Compound
1	274.5595	-
2	588.7282	-
3	340.5990	Yohimbic acid/Behenic acid
4	397.2072	-
5	274.5595	-
6	207.4622	-
7	277.4959	Convolidine/Venlafaxine
8	279.4951	Roemerine
9	291.5532	-
10	307.5475	Conviline/Foliosidine
11	293.5525	-
12	291.4908	Penbutolol
13	263.5013	Glycocitridine
14	299.5504	Komarovicine
15	293.4901	-
16	463.6904	-
17	295.5518	-
18	413.5778	Narcotine/ Solasodine
19	307.4850	Betaxolol/ Conviline
20	605.7879	-

Table 3. The LC-MS/MS analysis of sample 3 of *C. paniculatum*

Peak	m/z	Identified Compound
1	137.3090	-
2	207.3997	Salsolidine
3	197.3418	3,4-Dihydroxy-L-phenylalanine/Beclamide
5	397.2072	-
6	453.7552	-
7	281.4319	Coumarin 106/Cycloheximide
8	351.5331	Retrorsine
9	274.5595	-
10	288.5544	Testosterone
12	304.6111	9,10,16-Trihydroxyhexadecanoic acid/Tschimganin
14	322.6049	-
15	471.6886	-
16	324.6042	Glabranin/Quinine
17	569.7314	-
18	326.6036	Ajmaline/ <i>N</i> -Methylisothobainium
19	256.5665	alpha-Dihydrolysergol
20	313.5455	Heliotrine
21	639.5952	-
22	341.5987	-
23	152.3636	Ribitol
24	797.8255	-
25	131.6870	-

Molecular Docking Stage

The potential activity of the compounds analyzed by LC-MS/MS in inhibiting the 3CL protease of SARS-CoV-2 became one of our targets to accelerate the drug discovery process and predict the interaction between ligands and receptors at the molecular level. The molecular structures of baicalein, komarovicine, and roemerine are presented in Fig. 1. The docking study was applied by validating the docking process to the active site of this protease based on the RMSD parameters. The docking parameter had an RMSD of 0.723 Å (Fig. 2(a)) after the baicalein conformation from re-docking process was superimposed onto its X-ray conformation. Baicalein complexed with 3CL protease was chosen because it has drug-like characteristics that are commonly used as protease inhibitors. The docking results identified three compounds (komarovicine, roemerine, and solasodine) with lower binding energies than baicalein (-31.38 kJ/mol). These two compounds have binding energies similar to baicalein, namely coumarin-106 and

glabranin. Komarovicine has the lowest binding energy of -33.47 kJ/mol, followed by roemerine and solasodine at -32.63 and -32.21 kJ/mol, respectively.

In Baicalein, hydrogen bonds with Glu166 on the carbonyl group and Gly143 with hydroxyl groups on the

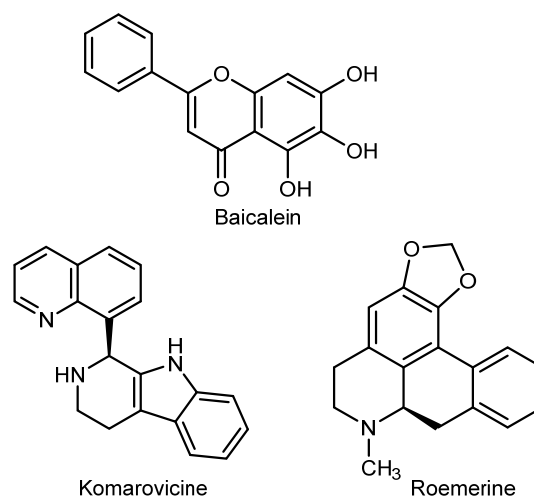


Fig 1. The molecular structures of baicalein and best-docked compounds

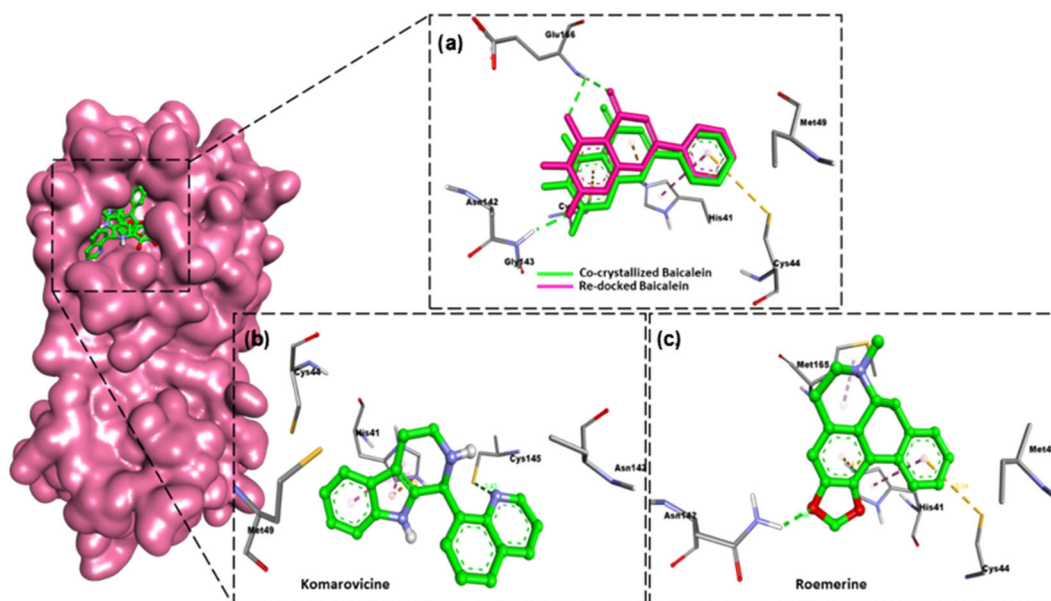


Fig 2. Molecular interactions of best compounds in the *C. paniculatum* fraction with 3CL protease of SARS-CoV-2. (a) overlay 3D conformation of co-crystallized and docked baicalein, 2D interactions of (b) komarovicine, and (c) roemerine with 3CL protease of SARS-CoV-2

chroman ring were observed. In addition, there is also a carbon-hydrogen bond with the Cys145 residue and a pi-donor hydrogen bond with the Asn142 residue. Hydrophobic interactions were formed at the His41 and Met49 residues (Fig. 2(a)). Meanwhile, komarovicine formed a hydrogen bond with Cys145 on the nitrogen atom of its quinoline ring (Fig. 2(b)). Interestingly, pi-donor hydrogen bonds with Asn142 residues and hydrophobic interactions with Cys44 and Met49 residues were observed in this compound. In roemerine, hydrogen bonds were formed at residues Glu166 with a carbon-hydrogen bond type and Asn 142, which is similar to

baicalein (Fig. 2(c)). This compound had hydrophobic interactions similar to those of other compounds but differed only in the Met165 residue.

Molecular Dynamics Simulation

The RMSD and RMSF analysis

RMSD analysis of the protease system and its ligands (baicalein, komarovicine, and roemerine) is presented in Fig. 3(a). The results show that the baicalein RMSD increased to 0.28 nm at 40–70 ns simulation time. A similar trend was also observed for roemerine at 80–90 ns, which moved higher to 0.32 nm but then decreased

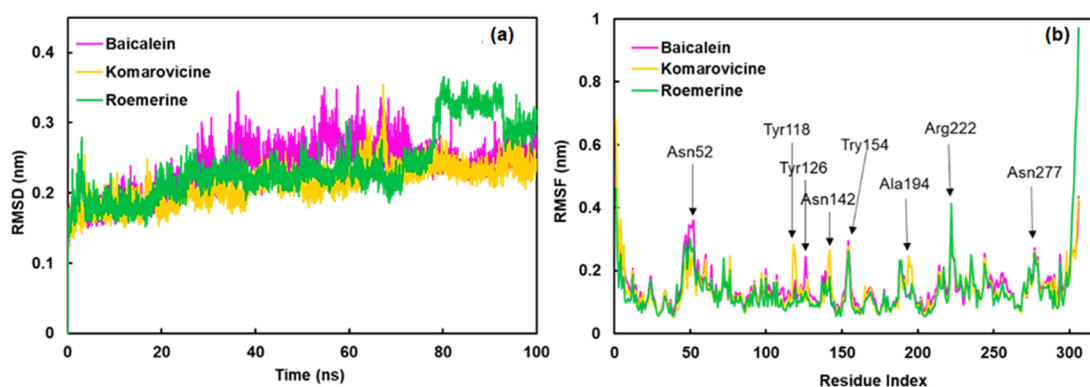


Fig 3. The plots of (a) RMSD of backbone atoms for protease complex, and (b) RMSF of backbone atoms for protease complex, during 100 ns of simulation

to 0.29 nm until the end of the simulation. Overall, komarovicin was relatively more stable than baicalein and roemerine, with a mean value of 0.237 nm.

RMSF analysis of the protease backbone region showed that all complexes had similar flexibilities (Fig. 3(b)). Several residues with high RMSF values included Asn52, Tyr118, Tyr126, Asn142, Tyr154, Ala194, Arg222, and Asn277. The Gln306 residue in the protease loop region showed very high peak fluctuations for roemerine at 0.97 nm and other compounds at 0.42 nm. Fluctuations in the Asn52 and Tyr126 residues of the baicalein complex were higher than those in the other two compounds, at 0.36 and 0.24 nm, respectively. Lastly, komarovicine showed more active fluctuations than other compounds, such as Try119, Asn142, and Ala194 residues, with 0.28, 0.26, and 0.24 nm, respectively.

Radius of gyration and principal component analysis

The compactness of the protease during the simulation was determined by measuring the Rg (Fig. 4(a)). Rg values in the low range indicated that the protease folded at a stable level. It can be seen in the graph that the protease complex with komarovicine and roemerine had similar compactness from the beginning to the end of the

simulation, with an average Rg value of ~2.225 nm. Unlike other compounds, the baicalein complex had a high Rg 2.25 nm at a simulation time of 40–100 ns.

We analyzed the overall essential dynamic patterns of the complex using PCA. Protein movement was recorded using two eigenvectors and visualized using a Cartesian plot (Fig. 4(b)). A stable complex can be identified from the smaller space occupied by the cluster during simulation. The roemerine complex occupied less space than the other complexes, but it appeared similar to the komarovicine complex. In contrast to the other complexes, baicalein demonstrated the most significant atomic movement of the protein.

Binding energy calculations

We analyzed the binding energies by applying the MM-PBSA method to compare the affinities of each complex system. The binding energies (ΔE_{BIND}) can be seen in Table 4.

The variables affecting the binding affinity of the complexes were investigated including the van der Waal energy (ΔE_{VDW}), electrostatic (ΔE_{ELE}), polar solvation (ΔE_{PB}), and solvent-accessible surface area energy (ΔE_{SASA}). Baicalein, as a standard, had a binding energy

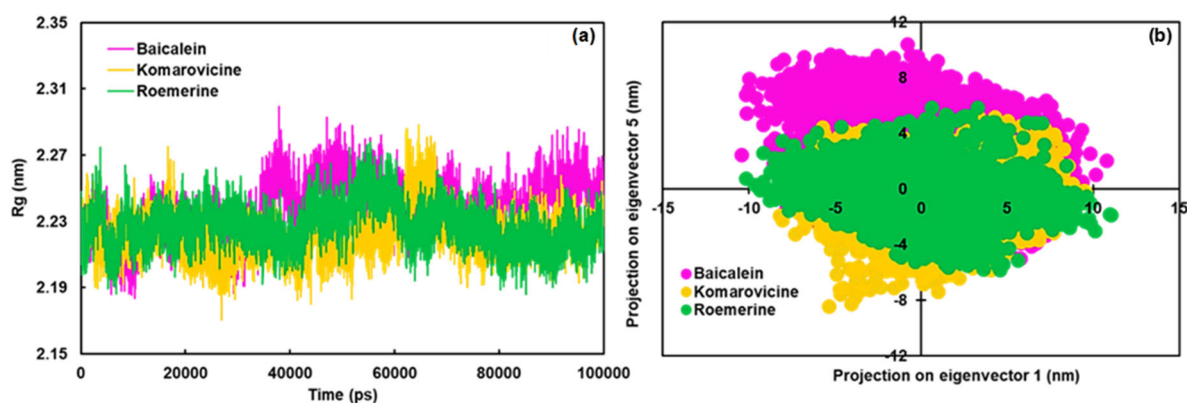


Fig 4. The plots of (a) radius of gyration of backbone atoms for protease complex, and (b) principal component analysis of the projected trajectory in 2D, during 100 ns of simulation

Table 4. Binding energy prediction by the MM-PBSA method*

Compounds	ΔE_{VDW}	ΔE_{ELE}	ΔE_{PB}	ΔE_{SASA}	ΔE_{BIND}
Baicalein	-143.66 ± 14.48	-43.60 ± 8.71	135.59 ± 14.61	-13.61 ± 0.74	-65.28 ± 15.99
Komarovicine	-71.13 ± 27.76	-12.17 ± 9.02	55.39 ± 43.62	-8.61 ± 2.78	-36.53 ± 41.93
Roemerine	-135.85 ± 16.20	-7.84 ± 6.40	67.47 ± 14.66	-13.21 ± 1.33	-89.44 ± 11.94

*All values are in kJ/mol

of -65.28 kJ/mol, which is higher than roemerine (-89.44 kJ/mol). Meanwhile, komarovicine showed higher energy than baicalein, with a value of -36.53 kJ/mol, due to the complex's lack of van der Waals interactions. These results demonstrated the ability of the *C. paniculatum* fraction to inhibit the 3CL protease of SARS-CoV-2. The analysis showed that the van der Waals energy had the most significant contribution to the binding affinity. On the other hand, the polar solvation energy is less favorable for complex systems.

In Vitro Inhibition Assay on 3CL Protease of SARS-CoV-2

Three sample fractions of *C. paniculatum* leaves (samples 1, 2, 3) were tested for their inhibitory ability against the 3CL protease enzyme from SARS-CoV-2 (Fig. 5). The measurement results for each sample were then compared with those of the positive control, GC376. This assay showed that all samples had similar inhibitory activities, but were slightly less active than GC376. This test was carried out by measuring the fluorescence intensity of the mixture (sample, substrate, and enzyme), where a lower intensity indicates the ability of the sample to inhibit 3CL protease activity. FRET is a vulnerable method for measuring molecular dissociation [40]. FRET works by transferring non-radiative energy from one excited fluorophore (donor) to a chromophore (acceptor), producing an absorption signal at a specific wavelength [41].

Interestingly, sample 2 inhibited the 3CL protease by 94.30%, which was close to the positive control's inhibition value of 98.19%. Based on these results, this enzyme could only change the substrate by 5.7% due to inhibition by sample 2. Sample 1 had 89.64%, a lower inhibitory activity than sample 2. Sample 3 had the lowest inhibitory activity (85.24%). The *C. paniculatum* leaves fraction inhibited the activity of 3CL protease and showed potential as an anti COVID-19 agent. The isolation of the active compounds and more detailed testing of this plant fraction are still auspicious for the development of COVID-19 drugs.

Several studies have reported the biological activity

of *C. paniculatum*; for example, Poriferasta-5,22E,25-trien-3 β -ol from its leaf inhibited 82% of Cucumber Mosaic Virus (CMV) activity at a concentration of 300 ppm [42]. Petroleum ether and chloroform extracts from this plant showed reduced inflammation in *in vitro* and *in vivo* assays at doses of 200 and 400 mg/kg compared to indomethacin (10 mg/kg) [43]. In addition, *C. paniculatum* root extract was highly antimutagenic in an *in vitro* assay against frameshift and base substitution mutations caused by nitrite-treated 1-aminopyrene [24]. The antiviral activity of *C. paniculatum* has not been extensively studied. However, the other families, such as *C. serratum*, which effectively inhibit yellow fever virus (EC_{50} = 15.9 mcg/mL) [44] and root extract of *C. myricoides*, can reduce the spread of human respiratory syncytial virus infection with EC_{50} = 0.21 mcg/mL [26]. Taraxero compounds from *Clerodendrum* spp. by computational studies with molecular dynamics were predicted to inhibit the main protease, RdRp, and spike protein of SARS-CoV-2 [45]. A docking study conducted by Erukainure et al. [46] revealed that the compound harpagide 5-O- β -D-glucopyranoside from *C. volubile* interacts and binds strongly at the initiation of translation and termination of mRNA sequence sites on the SARS-CoV-2 S-protein and ACE-2 receptor. To our knowledge, the *in vitro* assay of *C. paniculatum* against the SARS-CoV-2 protease in this study is the first to be reported.

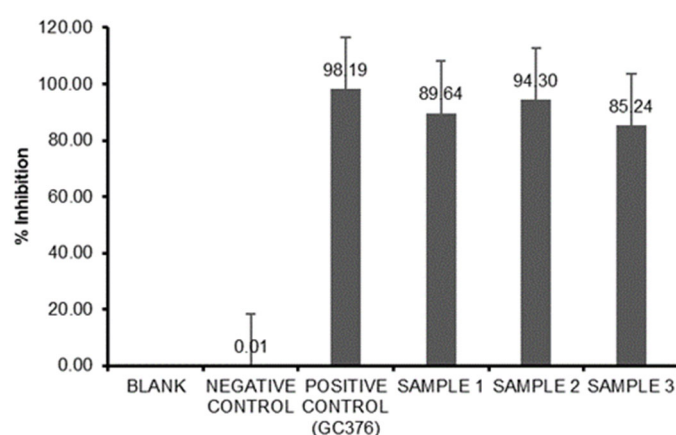


Fig 5. The percent inhibition activity of *C. paniculatum* fractions and GC376 against 3CL protease of SARS-CoV-2 by *in vitro* assay

■ CONCLUSION

LC-MS/MS and computational studies have identified potential compounds from the leaf fraction of *C. paniculatum* as 3CL protease inhibitors of SARS-CoV-2. Roemerine and komarovicine, which are alkaloid compounds from this plant, show a more optimistic binding energy prediction than baicalein. Roemerine was able to stabilize and bind strongly to proteases during simulation based on trajectory analysis of the backbone dynamics of the proteases. The *in vitro* assay successfully determined the potential of this plant fraction as a 3CL protease inhibitor of SARS-CoV-2. Sample 2 had an inhibitory activity of 94.30%, which was slightly lower than that of the positive control, GC376 (98.19%). Furthermore, samples 1 and 3 had perfect inhibitory activities of 89.64% and 85.24%, respectively.

■ ACKNOWLEDGMENTS

Muhammad Arba would like to thank the late Dr. Maywan Hariono for helping the *in vitro* assay.

■ AUTHOR CONTRIBUTIONS

Muhammad Arba conducted the experiment and wrote and revised the manuscript, Arfan conducted the MD simulation, Yamin conducted extraction and fractionation, Muhammad Sulaiman Zubair wrote and revised the manuscript. All authors agreed to the final version of this manuscript.

■ REFERENCES

- [1] Kumar, A., Singh, R., Kaur, J., Pandey, S., Sharma, V., Thakur, L., Sati, S., Mani, S., Asthana, S., Sharma, T.K., Chaudhuri, S., Bhattacharyya, S., and Kumar, N., 2021, Wuhan to world: The COVID-19 pandemic, *Front. Cell. Infect. Microbiol.*, 11, 596201.
- [2] Adil, M.T., Rahman, R., Whitelaw, D., Jain, V., Al-Ta'an, O., Rashid, F., Munasinghe, A., and Jambulingam, P., 2021, SARS-CoV-2 and the pandemic of COVID-19, *Postgrad. Med. J.*, 97 (1144), 110–116.
- [3] Djalante, R., Lassa, J., Setiamarga, D., Sudjatma, A., Indrawan, M., Haryanto, B., Mahfud, C., Sinapoy, M.S., Djalante, S., Rafliana, I., Gunawan, L.A., Surtiari, G.A.K., and Warsilah, H., 2020, Review and analysis of current responses to COVID-19 in Indonesia: Period of January to March 2020, *Prog. Disaster Sci.*, 6, 100091.
- [4] Aisyah, D.N., Mayadewi, C.A., Diva, H., Kozlakidis, Z., Siswanto, S., and Adisasmito, W., 2020, A spatial-temporal description of the SARSCoV-2 infections in Indonesia during the first six months of outbreak, *PLoS One*, 15 (12), e0243703.
- [5] Jensen, H.I., Ozden, S., Kristensen, G.S., Azizi, M., Smedemark, S.A., and Mogensen, C.B., 2021, Limitation of life-sustaining treatment and patient involvement in decision-making: a retrospective study of a Danish COVID-19 patient cohort, *Scand. J. Trauma, Resusc. Emerg. Med.*, 29 (1), 173.
- [6] Gottlieb, R.L., Vaca, C.E., Paredes, R., Mera, J., Webb, B.J., Perez, G., Oguchi, G., Ryan, P., Nielsen, B.U., Brown, M., Hidalgo, A., Sachdeva, Y., Mittal, S., Osiyemi, O., Skarbinski, J., Juneja, K., Hyland, R.H., Osinusi, A., Chen, S., Camus, G., Abdelghany, M., Davies, S., Behenna-Renton, N., Duff, F., Marty, F.M., Katz, M.J., Ginde, A.A., Brown, S.M., Schiffer, J.T., and Hill, J.A., 2022, Early remdesivir to prevent progression to severe Covid-19 in outpatients, *N. Engl. J. Med.*, 386 (4), 305–315.
- [7] Patel, T.K., Patel, P.B., Barvaliya, M., Saurabh, M.K., Bhalla, H.L., and Khosla, P.P., 2021, Efficacy and safety of lopinavir-ritonavir in COVID-19: A systematic review of randomized controlled trials, *J. Infect. Public Health*, 14 (6), 740–748.
- [8] Gautret, P., Lagier, J.C., Honoré, S., Hoang, V.T., Colson, P., and Raoult, D., 2021, Hydroxychloroquine and azithromycin as a treatment of COVID-19: Results of an open label non-randomized clinical trial revisited, *Int. J. Antimicrob. Agents*, 57 (1), 106243.
- [9] Salazar, E., Perez, K.K., Ashraf, M., Chen, J., Castillo, B., Christensen, P.A., Eubank, T., Bernard, D.W., Eagar, T.N., Long, S.W., Subedi, S., Olsen, R.J., Leveque, C., Schwartz, M.R., Dey, M., Chavez-East, C., Rogers, J., Shehabeldin, A., Joseph, D., Williams, G., Thomas, K., Masud, F., Talley, C., Dlouhy, K.G., Lopez, B.V., Hampton, C., Lavinder,

- J., Gollihar, J.D., Maranhao, A.C., Ippolito, G.C., Saavedra, M.O., Cantu, C.C., Yerramilli, P., Pruitt, L., and Musser, J.M., 2020, Treatment of coronavirus disease 2019 (COVID-19) patients with convalescent plasma, *Am. J. Pathol.*, 190 (8), 1680–1690.
- [10] Izcovich, A., Siemieniuk, R.A., Bartoszko, J.J., Ge, L., Zeraatkar, D., Kum, E., Qasim, A., Khamis, A.M., Rochweg, B., Agoritsas, T., Chu, D.K., McLeod, S.L., Mustafa, R.A., Vandvik, P., and Brignardello-Petersen, R., 2022, Adverse effects of remdesivir, hydroxychloroquine and lopinavir/ritonavir when used for COVID-19: Systematic review and meta-analysis of randomised trials, *BMJ Open*, 12 (3), e048502.
- [11] Mody, V., Ho, J., Wills, S., Mawri, A., Lawson, L., Ebert, M.C.C.J.C., Fortin, G.M., Rayalam, S., and Taval, S., 2021, Identification of 3-chymotrypsin like protease (3CLPro) inhibitors as potential anti-SARS-CoV-2 agents, *Commun. Biol.*, 4 (1), 93.
- [12] Osipiuk, J., Azizi, S.A., Dvorkin, S., Endres, M., Jedrzejczak, R., Jones, K.A., Kang, S., Kathayat, R.S., Kim, Y., Lisnyak, V.G., Maki, S.L., Nicolaescu, V., Taylor, C.A., Tesar, C., Zhang, Y.A., Zhou, Z., Randall, G., Michalska, K., Snyder, S.A., Dickinson, B.C., and Joachimiak, A., 2021, Structure of papain-like protease from SARS-CoV-2 and its complexes with non-covalent inhibitors, *Nat. Commun.*, 12 (1), 743.
- [13] Vlachakis, D., Papakonstantinou, E., Mitsis, T., Pierouli, K., Diakou, I., Chrousos, G., and Bacopoulou, F., 2020, Molecular mechanisms of the novel coronavirus SARS-CoV-2 and potential anti-COVID19 pharmacological targets since the outbreak of the pandemic, *Food Chem. Toxicol.*, 146, 111805.
- [14] Kanimozhi, G., Pradhapsingh, B., Singh Pawar, C., Khan, H.A., Alrokayan, S.H., and Prasad, N.R., 2021, SARS-CoV-2: Pathogenesis, molecular targets and experimental models, *Front. Pharmacol.*, 12, 638334.
- [15] Wu, C., Liu, Y., Yang, Y., Zhang, P., Zhong, W., Wang, Y., Wang, Q., Xu, Y., Li, M., Li, X., Zheng, M., Chen, L., and Li, H., 2020, Analysis of therapeutic targets for SARS-CoV-2 and discovery of potential drugs by computational methods, *Acta Pharm. Sin. B*, 10 (5), 766–788.
- [16] Gyebi, G.A., Ogunro, O.B., Adegunloye, A.P., Ogunyemi, O.M., and Afolabi, S.O., 2021, Potential inhibitors of coronavirus 3-chymotrypsin-like protease (3CL^{Pro}): An *in silico* screening of alkaloids and terpenoids from African medicinal plants, *J. Biomol. Struct. Dyn.*, 39 (9), 3396–3408.
- [17] Roe, M.K., Junod, N.A., Young, A.R., Beachboard, D.C., and Stobart, C.C., 2021, Targeting novel structural and functional features of coronavirus protease nsp5 (3CL^{Pro}, M^{Pro}) in the age of COVID-19, *J. Gen. Virol.*, 102 (3), 001558.
- [18] Malone, B., Urakova, N., Snijder, E.J., and Campbell, E.A., 2022, Structures and functions of coronavirus replication–transcription complexes and their relevance for SARS-CoV-2 drug design, *Nat. Rev. Mol. Cell Biol.*, 23 (1), 21–39.
- [19] Cannalire, R., Cerchia, C., Beccari, A.R., Di Leva, F.S., and Summa, V., 2022, Targeting SARS-CoV-2 proteases and polymerase for COVID-19 treatment: State of the art and future opportunities, *J. Med. Chem.*, 65 (4), 2716–2746.
- [20] Mathur, S., and Hoskins, C., 2017, Drug development: Lessons from nature, *Biomed. Reports*, 6 (6), 612–614.
- [21] Atanasov, A.G., Zotchev, S.B., Dirsch, V.M., Orhan, I.E., Banach, M., Rollinger, J.M., Barreca, D., Weckwerth, W., Bauer, R., Bayer, E.A., Majeed, M., Bishayee, A., Bochkov, V., Bonn, G.K., Braidy, N., Bucar, F., Cifuentes, A., D’Onofrio, G., Bodkin, M., Diederich, M., Dinkova-Kostova, A.T., Efferth, T., El Bairi, K., Arkells, N., Fan, T.P., Fiebich, B.L., Freissmuth, M., Georgiev, M.I., Gibbons, S., Godfrey, K.M., Gruber, C.W., Heer, J., Huber, L.A., Ibanez, E., Kijjoo, A., Kiss, A.K., Lu, A., Macias, F.A., Miller, M.J.S., Mocan, A., Müller, R., Nicoletti, F., Perry, G., Pittalà, V., Rastrelli, L., Ristow, M., Russo, G.L., Silva, A.S., Schuster, D., Sheridan, H., Skalicka-Woźniak, K., Skaltsounis, L., Sobarzo-Sánchez, E., Brecht, D.S., Stuppner, H., Sureda, A., Tzvetkov, N.T., Vacca, R.A., Aggarwal, B.B., Battino, M., Giampieri, F., Wink, M., Wolfender,

- J.L., Xiao, J., Yeung, A.W.K., Lizard, G., Popp, M.A., Heinrich, M., Berindan-Neagoie, I., Stadler, M., Daglia, M., Verpoorte, R., and Supuran, C.T., 2021, Natural products in drug discovery: Advances and opportunities, *Nat. Rev. Drug Discovery*, 20 (3), 200–216.
- [22] Shruthi, G., Joyappa, M.P., Chandrashekhar, S., Kollur, S.P., Prasad, M.N.N., Prasad, A., and Shivamallu, C., 2016, Bactericidal property of *Clerodendrum paniculatum* and *Saraca asoka* against multidrug resistant bacteria, restoring the faith in herbal medicine, *Int. J. Pharm. Sci. Res.*, 8 (9), 3863–3871.
- [23] Kopilakkal, R., Chanda, K., and Balamurali, M.M., 2021, Hepatoprotective and antioxidant capacity of *Clerodendrum paniculatum* flower extracts against carbon tetrachloride-induced hepatotoxicity in rats, *ACS Omega*, 6 (40), 26489–26498.
- [24] Phuneerub, P., Limpanasithikul, W., Palanuvej, C., and Ruangrunsi, N., 2015, *In vitro* anti-inflammatory, mutagenic and antimutagenic activities of ethanolic extract of *Clerodendrum paniculatum* root, *J. Adv. Pharm. Technol. Res.*, 6 (2), 48–52.
- [25] Prashith Kekuda, T.R., and Sudharshan, S.J., 2018, Ethnobotanical uses, phytochemistry and biological activities of *Clerodendrum paniculatum* L. (Lamiaceae): A comprehensive review, *J. Drug Delivery Ther.*, 8 (5), 28–34.
- [26] Umereweneza, D., Molel, J.T., Said, J., Atilaw, Y., Muhizi, T., Trybala, E., Bergström, T., Gogoll, A., and Erdélyi, M., 2021, Antiviral iridoid glycosides from *Clerodendrum myricoides*, *Fitoterapia*, 155, 105055.
- [27] Nallusamy, S., Mannu, J., Ravikumar, C., Angamuthu, K., Nathan, B., Nachimuthu, K., Ramasamy, G., Muthurajan, R., Subbarayalu, M., and Neelakandan, K., 2021, Exploring phytochemicals of traditional medicinal plants exhibiting inhibitory activity against main protease, spike glycoprotein, RNA-dependent RNA polymerase and non-structural proteins of SARS-CoV-2 through virtual screening, *Front. Pharmacol.*, 12, 667704.
- [28] Yamin, Y., Ruslin, R., Sartinah, A., Ihsan, S., Kasmawati, H., Suryani, S., Andriyani, R., Asma, A., Adjeng, A.N.T., and Arba, M., 2020, Radical scavenging assay and determination flavonoid and phenolic total of extract and fractions of Raghu bark (*Dracontomelon dao* (Blanco) Merr), *Res. J. Pharm. Technol.*, 13 (5), 2335–2339.
- [29] Su, H., Yao, S., Zhao, W., Li, M., Liu, J., Shang, W., Xie, H., Ke, C., Hu, H., Gao, M., Yu, K., Liu, H., Shen, J., Tang, W., Zhang, L., Xiao, G., Ni, L., Wang, D., Zuo, J., Jiang, H., Bai, F., Wu, Y., Ye, Y., and Xu, Y., 2020, Anti-SARS-CoV-2 activities *in vitro* of Shuanghuanglian preparations and bioactive ingredients, *Acta Pharmacol. Sin.*, 41 (9), 1167–1177.
- [30] Morris, G.M., Huey, R., Lindstrom, W., Sanner, M.F., Belew, R.K., Goodsell, D.S., and Olson, A.J., 2009, AutoDock4 and AutoDockTools4: Automated docking with selective receptor flexibility, *J. Comput. Chem.*, 30 (16), 2785–2791.
- [31] Arfan, A., Muliadi, R., Malina, R., Trinovitasari, N., and Asnawi, A., 2022, Docking and dynamics studies: Identifying the binding ability of quercetin analogs to the ADP-ribose phosphatase of SARS CoV-2, *Jurnal Kartika Kimia*, 5 (2), 145–151.
- [32] Trott, O., and Olson, A.J., 2010, AutoDock Vina: Improving the speed and accuracy of docking with a new scoring function, efficient optimization, and multithreading, *J. Comput. Chem.*, 31 (2), 455–461.
- [33] Abraham, M.J., Murtola, T., Schulz, R., Páll, S., Smith, J.C., Hess, B., and Lindahl, E., 2015, GROMACS: High performance molecular simulations through multi-level parallelism from laptops to supercomputers, *SoftwareX*, 1-2, 19–25.
- [34] Petrov, D., and Zagrovic, B., 2014, Are current atomistic force fields accurate enough to study proteins in crowded environments?, *PLoS Comput. Biol.*, 10 (5), e1003638.
- [35] Sousa da Silva, A.W., and Vranken, W.F., 2012, ACPYPE - AnteChamber PYthon Parser interfacE, *BMC Res. Notes*, 5 (1), 367.
- [36] Arba, M., Ruslin, R., Kalsum, W.U., Alroem, A., Muzakkar, M.Z., Usman, I., and Tjahjono, D.H., 2018, QSAR, molecular docking and dynamics studies of quinazoline derivatives as inhibitor of phosphatidylinositol 3-kinase, *J. Appl. Pharm. Sci.*, 8 (5), 1–9.

- [37] Wang, H., Gao, X., and Fang, J., 2016, Multiple staggered mesh Ewald: Boosting the accuracy of the smooth particle mesh Ewald method, *J. Chem. Theory Comput.*, 12 (11), 5596–5608.
- [38] Kumari, R., Kumar, R., and Lynn, A., 2014, *g-mmpbsa*—A GROMACS tool for high-throughput MM-PBSA calculations, *J. Chem. Inf. Model.*, 54 (7), 1951–1962.
- [39] Zubair, M.S., Maulana, S., Widodo, A., Pitopang, R., Arba, M., and Hariono, M., 2021, GC-MS, LC-MS/MS, docking and molecular dynamics approaches to identify potential SARS-CoV-2 3-chymotrypsin-like protease inhibitors from *Zingiber officinale* Roscoe, *Molecules*, 26 (17), 5230.
- [40] Liu, L., He, F., Yu, Y., and Wang, Y., 2020, Application of FRET biosensors in mechanobiology and mechanopharmacological screening, *Front. Bioeng. Biotechnol.*, 8, 595497.
- [41] Cihlova, B., Huskova, A., Böserle, J., Nencka, R., Boura, E., and Silhan, J., 2021, High-throughput fluorescent assay for inhibitor screening of proteases from RNA viruses, *Molecules*, 26 (13), 3792.
- [42] Musa, W., Hersanti, H., Zainuddin, A., and Tjokronegoro, R., 2009, The poriferasta compound-5,22e,25-trien-3-O β from *Clerodendrum paniculatum* leaf as inducer agent of systemic resistance on red chilli plant *Capsicum annum* L from Cucumber Mosaic Virus (CMV), *Indones. J. Chem.*, 9 (3), 479–486.
- [43] Joseph, J., Bindhu, A.R., and Aleykutty, N.A., 2013, *In vitro* and *in vivo* antiinflammatory activity of *Clerodendrum paniculatum* Linn. leaves, *Indian J. Pharm. Sci.*, 75 (3), 376–379.
- [44] Joshi, B., Panda, S.K., Jouneghani, R.S., Liu, M., Parajuli, N., Leyssen, P., Neyts, J., and Luyten, W., 2020, Antibacterial, antifungal, antiviral, and anthelmintic activities of medicinal plants of Nepal selected based on ethnobotanical evidence, *Evidence-Based Complementary Altern. Med.*, 2020, 1043471.
- [45] Kar, P., Sharma, N.R., Singh, B., Sen, A., and Roy, A., 2021, Natural compounds from *Clerodendrum* spp. as possible therapeutic candidates against SARS-CoV-2: An *in silico* investigation, *J. Biomol. Struct. Dyn.*, 39 (13), 4774–4785.
- [46] Erukainure, O.L., Atolani, O., Muhammad, A., Katsayal, S.B., Ebhuoma, O.O., Ibeji, C.U., and MESAİK, M.A., 2022, Targeting the initiation and termination codons of SARS-CoV-2 spike protein as possible therapy against COVID-19: The role of novel harpagide 5-O- β -D-glucopyranoside from *Clerodendrum volubile* P Beauv. (Labiatae), *J. Biomol. Struct. Dyn.*, 40 (6), 2475–2488.